

Article

Reliable Long-Range Multi-Link Communication for Unmanned Search and Rescue Aircraft Systems in Beyond Visual Line of Sight Operation

Johannes Güldenring *, Philipp Gorczak, Fabian Eckermann, Manuel Patchou,
Janis Tiemann, Fabian Kurtz and Christian Wietfeld

Communication Networks Institute (CNI), TU Dortmund University, 44227 Dortmund, Germany;
philipp.gorczak@tu-dortmund.de (P.G.); fabian.eckermann@tu-dortmund.de (F.E.);
manuel.mbankeu@tu-dortmund.de (M.P.); janis.tiemann@tu-dortmund.de (J.T.);
fabian.kurtz@tu-dortmund.de (F.K.); christian.wietfeld@tu-dortmund.de (C.W.)

* Correspondence: johannes.gueldenring@tu-dortmund.de

Received: 23 March 2020; Accepted: 25 April 2020; Published: 1 May 2020



Abstract: With the increasing availability of unmanned aircraft systems, their usage for search and rescue is close at hand. Especially in the maritime context, aerial support can yield significant benefits. This article proposes and evaluates the concept of combining multiple cellular networks for highly reliable communication with those aircraft systems. The proposed approach is experimentally validated in several unprecedented large-scale experiments in the maritime context. It is found that in this scenario, conventional methods do not suffice for reliable connectivity to the aircraft with significantly varying overall availabilities between 68% and 97%. The underlying work, however, overcomes the limitations of single-link connectivity by providing availability of up to 99.8% in the analyzed scenarios. Therefore, the approach and the experimental data presented in this work yield a solid contribution to search and rescue drones. All results and flight recording data sets are published along with this article to enable future related work and studies, external reproduction, and validation of the underlying results and findings.

Keywords: unmanned aircraft system (UAS); Unmanned Aerial Vehicle (UAV); search and rescue (SAR); long-range communications; Long-Term Evolution (LTE); Beyond Visual Line of Sight (BVLOS); multi-link; multi-path; multi-homing; multi-RAT; rescue robotics

1. Introduction

The recently growing availability and fast-paced development of Unmanned Aerial Vehicles (UAVs) have widened their area of application. One of these fields is the support of Search and Rescue (SAR) missions. When emergency calls are picked up in maritime rescue stations, time is the most critical parameter and every second counts. The success of SAR missions greatly depends on the information available to the rescue forces. The available knowledge about the situation, such as the position, is usually very imprecise and must be clarified as quickly as possible. Even though nowadays search and rescue strategies are highly developed, water-based searches by boat are slow and vessels may be unable to navigate in shallow waters or coastal areas. The aerial search typically relies on helicopters, which entail high costs. Moreover, flight operations and rescue missions are dangerous for the crew, especially under severe weather conditions. Unmanned Aircraft Systems (UASs) will close the gap and enable fast and safe detection of missing persons and ships.

The challenges of UAS usage in maritime SAR scenarios lie in the remote control as well as the real-time exchange of acquired information like sensor data, videos, and images. The former

two require low latency and high reliability, whereas the latter one conditions a real-time and high-throughput data flow. To tackle those challenges, the underlying publication proposes a holistic communication framework. The solution implements a multi-homing concept by using several Long Term Evolution (LTE) networks in parallel. This multi-link approach aims at mitigating minor break-ins or total failures of individual links and performing an aggregation to increase the overall throughput performance.

One major contribution of the underlying publication is the experimental validation in several unprecedented large-scale experiments, where all measurements and recorded datasets have been published (c.f. supplementary material at the end of this document). Therefore, the communication system has been implemented into a 3.6 m wide fixed-wing plane as part of the German national research project *LARUS* [1]. The implemented *LARUS* UAS for maritime SAR missions is the first civil project of its kind. A video demonstrating the capabilities of the UAS can be found in [2]. For the system evaluation, the UAS was launched from two airports located close to the coast at the Baltic sea in Germany and several flights were conducted. A schematic illustration of the scenario and the airport locations are depicted in Figure 1. The experiments consist of two parts: The first part primarily proofs feasibility and analyzes and evaluates connectivity as well as aerial maritime LTE channel parameters. The flights imitated realistic SAR scenarios and flight [2] accompanied one large-scale rescue simulation of the German Maritime Search and Rescue Association (German: “Deutsche Gesellschaft zur Rettung Schiffbrüchiger”, DGzRS). During those flights, real video payload was transferred between UAS and the local ground control and also used for the control of the UAS. In the second experiment series, the maximum performance of the communication was investigated. In order not to influence the video stream and flight control, a manned flight was conducted.

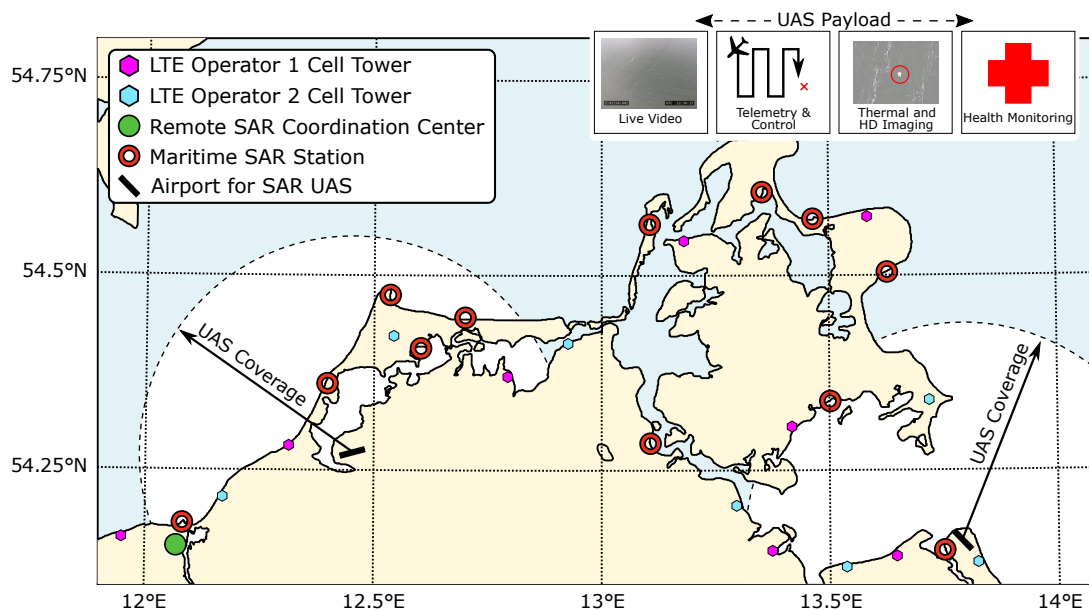


Figure 1. Schematic illustration of the Search and Rescue (SAR) scenario depicting the Unmanned Aircraft System (UAS) deployment at two different locations. The proposed multi-link approach leverages public cellular networks to transport live video, telemetry and control, and additional payload. The two depicted airports were actually used in the experimental validation in the remainder of this article.

The evaluations of the experiments show that the proposed solution significantly enhances communication quality. It is found that in the scenarios, conventional methods do not suffice for reliable connectivity to the aircraft with significantly varying overall availabilities between 68% and 97%. Leveraging multiple LTE networks overcomes the limitations of single-link connectivity by

providing an availability of up to 99.8%. Therefore, the approach and experimental data presented in this work yield a solid contribution to search and rescue drones.

In the following, the underlying work is structured as follows. First, relevant work is discussed and compared with the underlying approach in Section 2. Section 3 describes the system design, evaluation, and implementations, which were conducted to enable maritime UAV-based SAR operations. This is followed by a description of the evaluated scenarios and published datasets (Section 4). Finally, the flight experiments are evaluated and discussed in Sections 5–7. Section 6 highlights the benefits of the underlying multi-link approach.

2. Related Work

The sea provides a tough scenario due to its large search area and seclusion in connection with heavy wind and severe weather conditions. The need for fast, reliable, and safe exploration defines major research questions [3]. Missions are dangerous for manned vehicles, therefore the usage of robotics for safe operation is close at hand [4]. The concepts for the usage of UAVs for missing person detection [5] and drowning prevention [6] have been proposed in various publications [7]. Besides the major challenge of the detection, flight operation is another big issue. Even in fully autonomous flight operation, connectivity to the operator or other UAS and aerial traffic participants is necessary to control the operation and have suitable measures for collision avoidance. Challenges, like the UAV outback challenge [8], exist as incentives to tackle those challenges in a competition form with a fully integrated system.

Within the underlying work, we propose a holistic architecture and large-scale evaluation of all system aspects with the main focus on the air-to-ground communication link. A comparable UAV project is the *SEAGULL* [9], which targets maritime surveillance or vessel and shipwrecked tracking. However, the authors focus more on the person detection and fully autonomous flight operation. Unfortunately, the communication link is insufficiently described only as “UVH/SATCOM” link and lacks major details and evaluations. Another similar project is conducted in [10]. The authors propose a Beyond Visual Line of Sight (BVLOS) system for very-low level airspace. The communication link for reliable video and payload transfer consists of one public LTE and one wireless LAN in 2.4 GHz frequency band technology. In their work, the authors evaluate only the communication link in a ground-based experiment. The maximum achieved range is limited to 1.9 km, which is highly insufficient for maritime communication.

Enabling reliable and robust connectivity for air-to-ground communication is challenging due to the harsh environment and represents a key challenge of drone-based applications in disaster management [11]. The study [12] of the National Aeronautics and Space Administration (NASA) discusses methods and concepts for reliable UAV communication. The authors claim that the concept under which multiple service provider networks operate at the same time is fundamental and affords the best reliability, cost performance, and quality of service during the UAV’s flight. International Civil Aviation Organization (ICAO) currently considers integrating multi-link communication in its standards [13]. There are several conceptual, analytical and simulation-based studies for aerial connectivity exist. In [14], cellular connectivity for UAVs, as used throughout the underlying work, is described and analyzed in great detail.

Several competing protocols exist for the multi-link implementation. In following, the related work on combining multiple communications paths or links uses various terminology such as multi-path, multi-link, or multi-RAT (Radio Access Technology). We have chosen the term “multi-link” in order to capture both the radio- as well as protocol-related aspects of our work. Performance, maturity, and applicability between concepts and implementations vary significantly. Within the scope of this work, Multipath TCP (MPTCP) [15] is favored, which enables smooth handovers between different networks and communication links. MPTCP resides on the transportation layer and is transparent for the upper application layers. An overview and a comparison of multi-link protocols and their features are performed in the survey [16]. The comparison is based on Stream Control

Transmission Protocol (SCTP) [17], various SCTP extensions, and MPTCP. The study, which also conducts an empirical performance evaluation, results in favoring MPTCP as it provides the broadest feature set. A general performance evaluation of the benefits of vehicles, which are able to make use of up to three mobile communication networks, is performed in a preliminary study [18]. The proposed MPTCP transmits subflow configuration and sequence numbers as part of the Transmission Control Protocol (TCP) header. The Multi-Connection TCP (MCTCP) [19] proposes contrary behavior and uses several individual plain TCP connections for each network interface. It does not modify TCP itself but transmits the additional protocol overhead as part of the payload. Hereby, the protocol is able to mitigate the influence of middleboxes and firewalls, which may drop MPTCP's TCP-header modifications [20]. However, the protocol may behave unfairly to non-multi-link TCP connections as congestion control is uncoupled [21]. Other solutions are very application- or use case-specific: Maximum Multipath TCP (MMTCP) [22] provides a data center solution which significantly reduces the download time of short data flows, while at the same time providing high throughput for long data flows. Multipath UDP (MPUDP) [23] provides a multi-link transport protocol, based on User Datagram Protocol (UDP), which specializes and optimizes the usage of Virtual Private Networks (VPNs). ScalaNC [24] provides a Network Coding enhanced and UDP based solution for multi-link communication. Network coding, also in combination with MPTCP [25], can improve performance in scenarios with lossy communication links. However, due to the used cellular (4G/LTE) network, packet loss is not a major issue. Network coding also requires more computational overhead, which is unavailable on the embedded network platform.

For transmitting video payload over multiple parallel links several approaches exist in literature. The authors of [26] propose quALity-Driven Multipath TCP (ADMIT), which makes use of the MPTCP and applies a Forward Error Correction and rate allocation. Experimental results show that the algorithm outperforms reference protocols. A similar approach is used by Hayes et al. [27] proposing Dynamic Adaptive Streaming over HTTP (DASH). The approach benefits from using a lower video quality when the data rate is not sufficient. It induces an additional two-second latency on top of the data transfer and creates additional overhead by using Hypertext Transfer Protocol (HTTP)-based streaming. An improved data offloading is presented in [28], exchanging video latency against optimized data rate usage, which is also non-beneficial for the real-time video stream of the UAV. To solve the issue of uploading time-critical data, a deadline-constrained algorithm for video upload from vehicles has been proposed in [29]. The video is evaluated on traces. In [30], an empirical evaluation is performed on a proprietary multi-link transport layer protocol, but lacks a comparison to state-of-the-art transport layer protocols. The authors of [31] evaluate a UDP-based multi-link video transfer for remote vehicle control using a simulation, but lacks experimental evaluation.

To improve state-of-the-art networking and communication technologies, Google released the novel Quick UDP Internet Connections (QUIC) [32] protocol as part of the Chromium web browser [33]. QUIC is UDP-based and resides fully in the user-space. The first deployments on YouTube servers achieved good results and caused a growing interest in the protocol. This popularity led to two multi-link adoptions of Multipath QUIC (MPQUIC). The first implementation by Coninck et al. [34] provides the initial architecture and design for MPQUIC. The implementation is compared to MPTCP in an emulated static environment. For HTTP-based data transfers, MPQUIC tends to be slightly faster than MPTCP. However, the scenario seems beneficial to QUIC as it is optimized for HTTP and HTTP/2 traffic. In addition, mobility is not evaluated here. The second implementation of Viernickel et al. [35], which was developed in parallel, is also evaluated in a large-scale emulated experiment. For small HTTP/2 downloads (10–100 KB), MPQUIC seems to outperform MPTCP. For larger downloads (1 MB), both competitors meet at eye height, at high delay ratios MPTCP has a slightly better average (median) download time. The latter publication also provides a proof of concept by conducting a real-world experiment using an LTE modem and Wireless Local Area Network (WLAN) static setup. Device mobility has not been investigated. Even though both MPQUIC solutions provide promising results for future use in UAV communication, the implementations lack maturity and extensive field

tests in comparison to **MPTCP**. **MPQUIC** has only been tested in emulated and static scenarios. Therefore, **MPTCP** has been used throughout the experiments of this work. A trace-driven emulated evaluation of **MPQUIC** schedulers is provided in [36] and shows promising results of reduced latency. **MPTCP** has proven itself in several studies and investigations [37]. The authors of [38] successfully evaluate handovers between different networks in mobile scenarios. Simulations [39] using the *ns-2* network simulator promise 20% increases in throughput in **UAV** communication when using **MPTCP** over ad hoc wireless networks. Different extensions and modifications exist to improve **MPTCP** itself, the multi-link congestion control, or scheduling. ProgMP [40] provides an add-on, which enables the development of own application or preference aware **MPTCP** schedulers, e.g., a low latency **MPTCP** version [41].

The underlying maritime air-to-ground communication radio properties are described in several studies. The survey in [42] compares channel models especially with regard to their applicability in **UAV** communication. An accurate analytic description for the maritime air-to-ground links is provided by [43]. A long-range **LTE** communication in a maritime scenario over 180 km using a multi-cell approach, which is comparable to the public mobile communication networks in this paper, is performed in [44]. The authors have published empiric measurements of the received **LTE** radio power that enables a detailed channel description. A very detailed channel model has been developed by Matolak et al. [45]. In their work, the authors derive a two-ray channel model for maritime aerial description, which is founded on the groundwork of the authors of [46–48]. The model is enriched and parametrized by a large-scale measurement campaign using an aircraft. This model has been evaluated in a preliminary study of the authors of this publication in a multi-link scenario [49] and will be validated and referenced throughout the underlying work.

3. Proposed System Design, Architecture and Implementation

Several components and modules are required to enable the **UAS** to operate in **SAR** missions and stream live video data from the **UAV** to remote operators and stakeholders. Figure 2 provides an overview of the whole multi-link air-to-ground communication system architecture. The core component of the system is the LARUS aircraft. The **UAV** is equipped with one First-Person View (**FPV**) camera and one High Definition (**HD**) camera. The **FPV** camera provides a continuous video stream, which supports the drone operator on the ground in navigating the vehicle. The **HD** camera provides high-resolution pictures of the sea surface to find missing persons and perform **SAR** tasks. The camera is stabilized using a gimbal, which enables the rotation and movement of the camera by a remote operator in order to take pictures of areas of interest. In addition, the **UAV** is equipped with a monitoring module, which provides telemetry data (position, speed, altitude, etc.) and various health information (tank filling level, battery voltage, etc.). The **UAV** is equipped with three *Sierra Wireless MC7455* **LTE** modems to enable multi-link operation. Two of those modems are assigned to two public German Mobile Network Operators (**MNOs**), in the following referred to as **MNO 1** and **MNO 2**. The third modem is associated with an **LTE** small cell solution. This small cell solution supports the public **MNO** in proximity to the airport, where network coverage is not always given due to buildings and shadowing, and saves data volume during maintenance when the **UAV** is on the ground. In the future, a long-range **LTE** solution could serve as a drop-in replacement and assist the public **MNO**. All **UAV** components are connected via an embedded ARM-based computing platform. The platform runs a Linux operating system and uses an **MPTCP** kernel [50], which enables multi-link communication. Figure 3 shows a picture of the LARUS **UAV** plane. The **UAV** has a fixed wingspan of ~3.6 m and a total weight of ~26 kg. With its combustion engine, the **UAV** is able to fly for multiple hours and long distances. For communication, the public **LTE** antennas are located inside the tail fins of the aircraft. The right part of Figure 3 shows a cross-section of the front of the plane. Here resides the embedded multi-link platform as well as the dedicated **LTE** modem. Figure 4 shows the **UAS** during flight operation over the Baltic Sea.

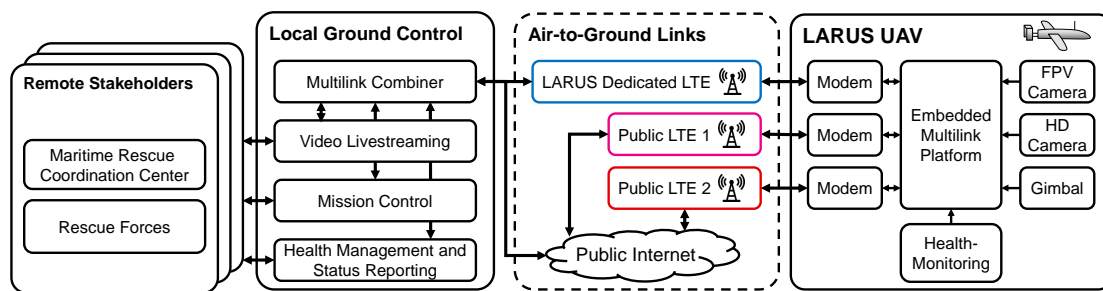


Figure 2. Architecture of the proposed multi-link communication.



Figure 3. Illustration of the LARUS Unmanned Aerial Vehicle (UAV) showing the location of the communication hardware in front and tail fin. The UAV has a fixed wingspan for 3.6 m and a total weight of 26 kg. With its combustion, engine it is able to fly for multiple hours. All experiments except flight [4] were performed with the pictured LARUS UAV. Images: © 2020 LARUS project [1].



Figure 4. The LARUS UAV during start (left) and during flight operation over the Baltic Sea near Ribnitz-Damgarten [2] (right). Images: © 2020 LARUS project [1].

The local ground control station is equipped with an off-the-shelf desktop computer, which also runs an [MPTCP](#) Linux kernel [50]. Here, the multi-link communication between UAV and ground control terminates. On the application layer runs a video live streaming platform, which makes use of [gstreamer](#) [51] for publishing and [Open Broadcaster Software Studio \(OBS Studio\)](#) [52] for video mixing. This video module provides a low latency video of the UAV FPV camera for the local drone operator. In addition, the video module supports rebroadcasting of the mixed stream via Real-Time Messaging Protocol (RTMP) to remote stakeholders, like rescue forces or the superior Maritime Rescue and Control Center (MRCC). The local ground control station is illustrated in Figure 5. It is located inside the white van. The dedicated LTE is mounted on the rooftop. Inside, the UAV can be tracked and controlled via various monitors. Figure 5 also shows an illustration of the LARUS control and health monitoring Graphical User Interface (GUI), where SAR missions can be conducted. The screenshot shows the Sector Search Pattern from flight experiment [3]. All data is made available to external stakeholders via a unified live video stream, for example, during Peenemünde flight experiment [3] (Final Demonstrator) rescue forces on a boat set out to save persons out of the water, were able to see live images provided

by the plane's cameras. In addition, the MRCC, which was located several hundred kilometers away, was able to interact with the mission control.

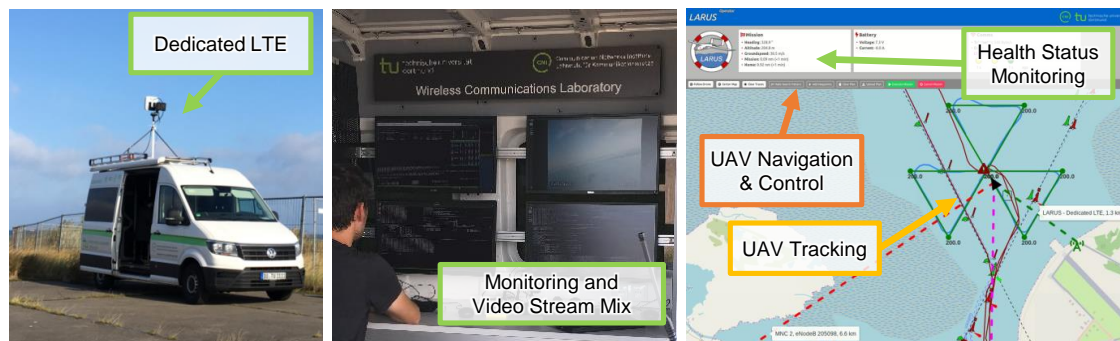


Figure 5. Illustration of the ground control station, which is located in the white van. The dedicated LTE is mounted on the rooftop. Inside, the LARUS aircraft is monitored and the final video stream mixed for external stakeholders.

During the UAV experiments, the video stream was used to navigate and monitor the vehicle. Maxing out the communication link's performance would have interfered with the video streaming. Therefore, an additional manned flight was conducted to assess the maximum key performance indicators of the system. The plane for the manned flight is illustrated in Figure 6. An ultra-lightweight plane was used for those experiments. The same hardware (antennas and multi-link platform) being used in the UAV experiments was also used during the manned flight to create comparable results. Due to the unavailability of space in the back, the antennas were placed at the front window of the plane, which is contrary to the UAV experiments.



Figure 6. In order to evaluate maximum performance without interfering video stream and telemetry and control data flows a manned flight was conducted. The illustration shows the used ultra-lightweight aircraft and antenna position of Peenemünde flight experiment [4].

4. Validation Scenarios and Published Datasets

The proposed UAS has been evaluated in several long- and short-range flight tests. To complement and round off the extensive UAS measurements a manned validation flight using a plane was undertaken. All flight tests were conducted at different locations and areas to demonstrate that the system is universally applicable and does not contain any spatial dependencies. Table 1 provides an overview of all available datasets. Within the scope of this work, all evaluations indicate the underlying data by referring to the numbering system [1] to [5] as defined in the table. In addition, Figure 7 shows a map and the trajectories of all flights.

Table 1. List of published and evaluated datasets.

Index	Location	Mission	Start	Stop
1	Peenemünde	Single Link	22 August 2019	07:17:54 22 August 2019 08:19:11
2a	Peenemünde	Long Range	14 September 2019	09:20:25 14 September 2019 10:04:34
2b	Peenemünde	SAR Mission	14 September 2019	10:15:25 14 September 2019 10:25:24
3	Peenemünde	Final Demonstrator	17 October 2019	11:58:32 17 October 2019 12:58:31
4a	Peenemünde	Manned Validation Flight 1	17 October 2019	11:58:32 17 October 2019 12:58:31
4b	Peenemünde	Manned Validation Flight 2	17 October 2019	11:58:32 17 October 2019 12:58:31
5	Ribnitz-Damgarten	Long Range	28 August 2019	14:07:58 28 August 2019 15:26:39

In the first evaluation area, the UAS was launched at Peenemünde airport (ICAO airport code EDCP). The trajectory of the flight is depicted in Figure 7a. Several flights originated from this location. The first data set 1 is a medium ranged flight with a maximum distance of 15 km above the island Greifswalder Oie. The focus of this flight was on hardware evaluation tests, therefore only a single-link communication was conducted. Data set 2 consists of two parts: In the first part 2a, a long-range distance flight in North–West direction was conducted, targeting the island Rügen. The altitude during the long-range flight was 400 m and the maximum distance between UAS and ground station was approx. 21 km. The flight tests accompanied a SAR exercise of the German maritime rescue forces. Therefore, in the following part 2b, the drone performed a *Creeping Line* search pattern exploring a rectangular area below the plane. Both datasets implement full multi-link communication. The chronologically following data set 3 contains measurements in the area around Peenemünde airport. A whole SAR scenario was conducted as part of the final project presentation of the LARUS project. Here, the UAS searched along the shore for a missing ship with a person floating on the open water. Having found the ship the UAS performed a *Sector Search* pattern, which is recognizable by the triangular-shaped trajectories. In the previous scenarios, the UAS communication links were used to transport and deliver mandatory telemetry, video imaging, and mission-related information. Therefore, the communication link’s limits could not be assessed without endangering and influencing the flight and mission performance. To complement and round off previous measurements, one manned validation experiment was carried out using a lightweight plane 4. Here, the communication link’s maximum throughput was quantified as well as network availability and roaming behavior in the proximity of the Polish–German border.

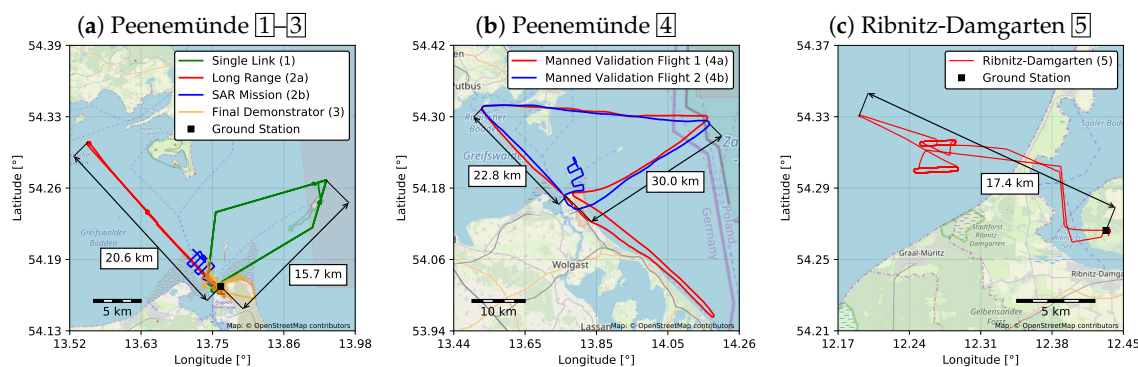


Figure 7. Trajectories of the test flights at two different locations in the Baltic Sea. Flights of dataset 4 were recorded using a manned plane, all other datasets (1–3 and 5) were conducted using the proposed SAR UAS (c.f. Figure 3).

The second location where flight experiments were conducted lies close to Ribnitz–Damgarten (Figure 7c), where the UAS was launched from the runway of an airport. The area turned out to be more challenging in terms of communication in comparison to the first location. After the launch, the UAS first needs to overfly the *Saaler Bodden*, a lagoon-like stretch of water, before reaching the seashore (see also Figure 1 for a large scale map). Moreover, the area is less populated along the flight direction

towards the Danish island *Falster*. Therefore, the mobile communication network deployment is sparse in the mentioned area.

5. Analysis of Public LTE Networks in Maritime Airspace

Using public LTE networks for aerial and maritime communication is challenging. MNOs usually optimize their LTE networks for ground users. Therefore, antennas at the cell tower are tilted downwards to achieve maximum gains and reduce interference with other cells. In addition, distances between enhanced NodeB (eNB) and User Equipment (UE) are larger. This results in worse radio channel conditions for aerial LTE users. Figure 8 highlights this issue by comparing the channel quality indicators of the Peenemünde flight data set [1] to a ground reference measurement. For channel quality, the UE-estimated Signal-to-Interference-plus-Noise Ratio (SINR) is analyzed. The received power is presented in form of the Reference Signal Received Power (RSRP). An estimate of the UE's power consumption is provided by the Transmission Power. The ground reference measurement was recorded during a drive test in a car on a German highway. The reference measurement uses the same LTE modem, antennas, and MNOs that were used in the aerial measurement campaign. The resulting figure shows the value distribution of each indicator incorporated by the Probability Density Function (PDF). For the aerial test, the SINR ranges from -10 to 5 dB with an average of -2.9 dB. The ground test results in a value range from -5 to 25 dB and a mean value of 13.5 dB. Besides the fact that aerial values are 16.4 dB below ground average, SINR values below 0 dB indicate the worst channel conditions. Communication needs to make use of the most robust modulation and coding schemes to successfully transmit data. Additionally, LTE's Hybrid Automatic Repeat Request (HARQ), which can recover packets that have not been successfully transmitted, supports the communication link. However, this results in a lower data rate and higher latency. If bad channel conditions cannot be fully compensated, side-effects will occur, from sporadic packet losses up to the whole communication link becoming unavailable. The poor channel quality is also recognizable in the received power. With a difference of 11.2 dB, the average aerial RSRP is significantly below the ground-based one. The difference is lower in comparison to the SINR because that the RSRP does include only the usable signal and no interference power levels. The UE uses more energy for aerial communications in terms of energy efficiency. The aerial data was transferred using an average of 20.4 dBm transmit power, whereas the ground reference transmitted on average 13.0 dBm, which is 7.4 dB less. Due to the limited resource availability in UAVs, the more than fivefold increased energy consumption must be taken into account when dimensioning power supplies.

Figure 9 illustrates the main channel quality indicators of the published datasets to provide an estimate of the channel quality over time. The figure references the same data as the preceding comparison of Figure 8. The highlighted indicators were recorded and published for each of the previously described flights. The received power is again represented using the Received Signal Strength Indicator (RSSI) and the RSRP, whereas SINR and Reference Signal Received Quality (RSRQ) are used for signal quality description. Figure 9 underlines the observations from the previous distributions of Figure 8. The RSSI is defined as the total power the UE observes in the whole used frequency band. Therefore, it incorporates signal power as well as noise and interferences. In addition, the RSRP measurements reflect the average linear power of a single reference carrier. Thus, it provides an estimate of the strength of the usable signal of the network. As it does not include interferences and noise, it lies clearly below the RSSI measurements. In the underlying time-series, the difference is on average 32 dB. RSRP measurements locally range down to nearly -100 dBm. Assuming a typical UE receiver noise floor of -97 dBm [53] underlines the challenges of maritime air-to-ground communication. The upper subplot shows the signal quality in terms of RSRQ and SINR. Both show a strong correlation.

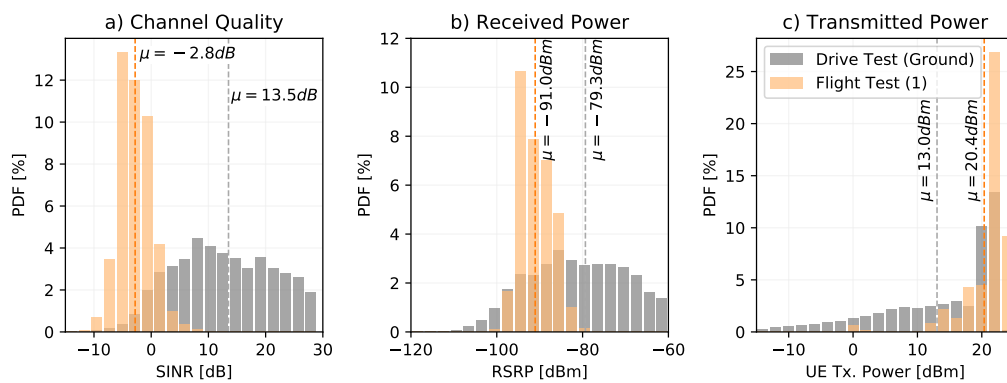


Figure 8. Challenges of aerial communication: public networks are optimized for ground users and antennas are usually tilted downwards. In addition to the larger distance between the cell tower of the serving enhanced NodeB (eNB) to User Equipment (UE), the experienced channel quality for UAS is significantly worse than for ground users. This figure compares the channel quality indicators Signal-to-Interference-plus-Noise Ratio (SINR), Reference Signal Received Power (RSRP), and UE Transmission Power of a Peenemünde flight test with a reference measurement, which was captured during a one-hour highway drive using a car. For each indicator, the aerial-based measurements are worse than ground reference measurements. MNO 1, Data set [1].

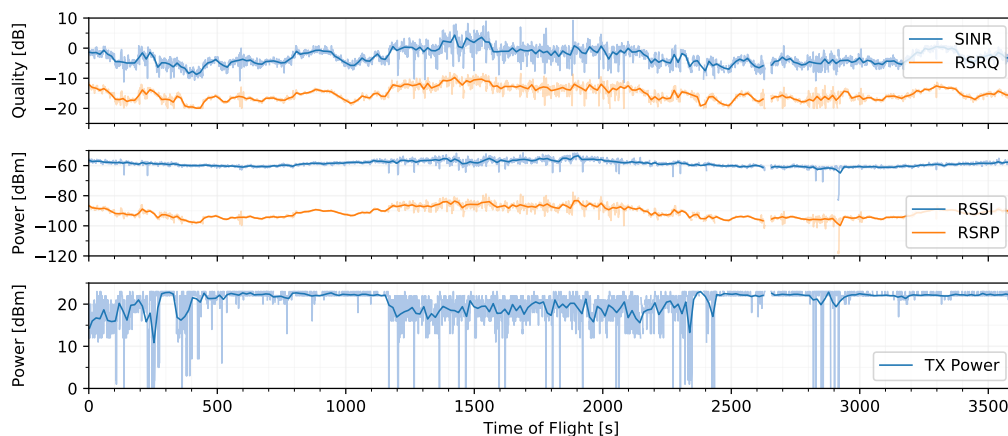


Figure 9. Time-series evaluation shows the main LTE radio channel indicators: Signal-to-Interference-plus-Noise Ratio (SINR) and Reference Signal Received Quality (RSRQ) for channel quality, Reference Signal Received Power (RSRP), and Received Signal Strength Indicator (RSSI) for received power and UE transmission power. MNO 1, Data set [1].

In order to analyze correlations and model channel conditions more precisely, Figure 10 compares the RSRQ to (a) RSSI, (b) RSRP, and (c) SINR in the form of a scatter plot. Moreover, the ground-based measurements serve as a comparative reference to the in-flight measurements. The evaluations underline the bad value range of the channel quality indicators. For RSSI, the value range lies between -50 dBm and -70 dBm. Data points lie on noisy lines, distinguishable by the used frequency. Even though the Pearson correlation coefficient (c.f. Table 2) ranges up to $\rho = 0.613$ for LTE Band 3, a direct derivation of RSRQ based only on RSSI measurements is not possible. The scatter plot Figure 10b of RSRQ and RSRP reveals a linear correlation with the Pearson coefficient being above $\rho \geq 0.88$ for all used frequency bands. Measurements of the reference signal power allow direct estimation of channel quality. This is contrary to the ground-based measurements, where nearly no correlation can be found, which is also confirmed by low correlation coefficients between 0.25 and 0.54. This is attributed to a lot of shadowing by buildings and obstacles, reflections, and multipath interferences, which occur during drive tests and perform a significant degradation of signal quality.

In summary, this leads to the conclusion that interferences with other LTE users and fast fading effects are neglectable. Channel quality is therefore mainly determined by path loss.

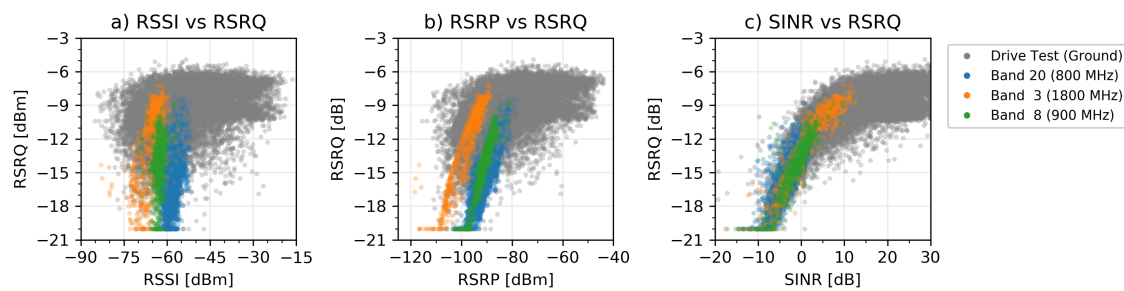


Figure 10. Scatter plots of in-flight recorded RSRQ and RSSI (a), RSRP (b), and SINR (c) measurements in comparison to a ground reference measurement. Linear correlation between channel indicators shows that only a few fast fading interferences and noise are present. Compare Table 2 for correlation coefficients. MNO 1 data sets [1][2][3].

Table 2. Pearson correlation coefficients of RSRQ (c.f. Figure 10).

	RSRQ Flight Tests			RSRQ Drive Test (Ground)		
	Band 3	Band 8	Band 20	Band 3	Band 8	Band 20
RSSI	0.613	0.281	0.430	0.070	n/a	0.400
RSRP	0.931	0.938	0.878	0.252	n/a	0.543
SINR	0.933	0.889	0.897	0.560	n/a	0.729

In the next step, the path loss effects are further investigated. To derive channel characteristics and evaluate signal attenuation, Figure 11 evaluates the received power in dependency of the distance between UE and the currently connected cell (eNB). The analysis leverages the received signal power (RSRP) of the three most frequently used eNBs in the 800 MHz frequency band (LTE Band 20). Different sectors of each eNB were consolidated in the evaluation as the according antennas are located at the same radio tower. The left subplot (a) illustrates the path loss and power, the right subplot (b) shows a map of the eNB locations and positions, where the RSRP samples were recorded. When discussing aerial communication, free space characteristics are usually assumed. Typically, there are no obstacles are between sender and receiver: the direct Line of Sight (LOS) assumption is valid. This aspect can be seen by the recorded RSRP samples of Cell Identifier (Cell ID) 1ED4B01 (green color). In the distance between 9 and 14 km, the signal strength decreases linearly with respect to the logarithmic distance. The free space path loss can be modeled using the Friis Transmission Equation [47] with the propagation coefficient γ . The propagation coefficient has a major impact on the path loss. For 1ED4B01 (green color), a propagation coefficient of $\gamma \approx 2.0$ holds true. An approximate Effective Isotropic Radiated Power (EIRP) of 30 dBm is estimated for the illustrated model. With increasing distance, the RSRP measurements diverge from the free space model and form uneven patterns even though the LOS condition is given. These effects can be explained using the maritime channel model (see previous work of the authors, where this model is discussed in detail [49,54]). In addition to the direct LOS path, the maritime channel model takes a secondary, ground-reflected Non-Line of Sight (NLOS) path into account. The superposition of multiple radio propagation paths leads to interferences causing the divergences from the free space path loss model. The illustrated maritime channel model in Figure 11 uses an estimated antenna height of 100 m and measured UAV altitude of 400 m. The model provides a good approximation of the measured RSRP. In the near field, the secondary NLOS path is blocked by ground-based obstacles (e.g., trees, buildings, etc.) and the maritime two-ray model does not apply. This can be seen in the map subplot especially for Cell ID 1ED4B01 (green). In the first 14 km, the NLOS is blocked and free space model applies.

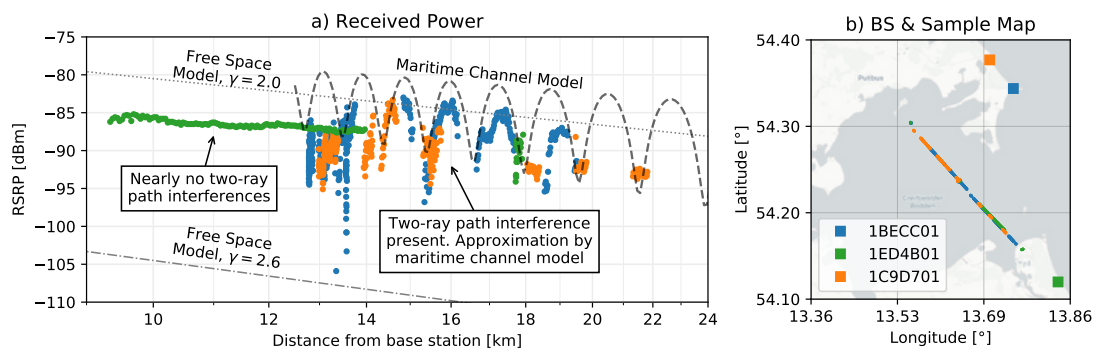


Figure 11. Received signal strength evaluation of the three most used LTE cells of MNO 1 during Peenemünde flight [2a]. Whereas the left plot (a) illustrates the signal strength in dependency of the UAS distance, the right illustration shows the eNB positions as well as the location, where samples were recorded. The signal of the eNB with cell id 1ED4B01 follows rural characteristics: there are no two-ray path interferences, and therefore the signal strength can be described using the free space model. The other two eNBs 1BECC01 and 1C9D701 have strong variances. These valleys can be described using the proposed maritime channel model. MNO 1, data set [2a].

Figure 12 illustrates the connectivity of the UAV to the different cells of each MNO during the first half of the Peenemünde long-range flight [2a]. The first column (subplots a,c) indicates the cell identifier to which the LTE modem of the UAV is currently connected to. The first five characters of the Cell ID represent the identifier of the eNB, the last two characters indicate different sectors or antennas of the same eNB. Within all figures, different antennas were grouped for each eNB and share the same colors. The upper row of the cell identifier plot shows the availability of the MNO. The availability represents whether the network was able to transport payload data. The detailed methodology for the determination of the availability will be discussed in detail in the subsequent section and Figure 13. Within Figure 12, the right column (b,d) shows a map of the locations of each eNB. The upper row (a,b) represents MNO 1 evaluations and the lower row (c,d) MNO 2 evaluations. During the first half hour of the flight, the UAV is connected to 21 different eNBs of MNO 1 and 25 eNBs of MNO 2. Throughout the flight, the UAV's LTE modem performs 111 handovers between cells of those eNBs, which correspond to an average length of stay of 16.2 s per cell for MNO 1. For MNO 2, 166 cell changes were conducted leading to an even smaller duration of stay of 10.8 s. Handovers in LTE are either initiated by the EPC or by the UE. However, the final handover decision remains at the core network and aims at maintaining and maximizing the user's Quality of Service (QoS) (c.f. also resource allocation in next-generation broadband wireless access networks [55]). Here, it is once again obvious that the decisions are optimized for ground users: handovers are conducted between unsuitable cells, which leads to a back-and-forth switching between two cells. This effect can be seen, e.g., at MNO 1 between cells 1ECD901 (purple) and 1D8C801 (black) (at time of flight 1300 s–1700 s) or between cells 1A6CF03 (pink), 1BECC02 (blue), and 18F9A01 (red) (1000 s–1300 s). Typically, the decision policies use the UE's measurement report, which indicates the quality of all cells the UE can see. In the underlying scenario, typically all cells have unfavorable channel conditions. For future work, we propose a mobility and maritime channel aware handover decision policy for UAVs. Hereby, handover decisions could be improved significantly. An additional optimization would be to disable frequency bands above 1 GHz. On a few occasions, the UEs were able to detect cells in LTE band 1 (2100 MHz) and band 7 (2600 MHz). Those cells typically have more bandwidth and most MNO aim at moving users there for improved load balancing. In the underlying maritime scenario, those handovers failed on a regular basis.

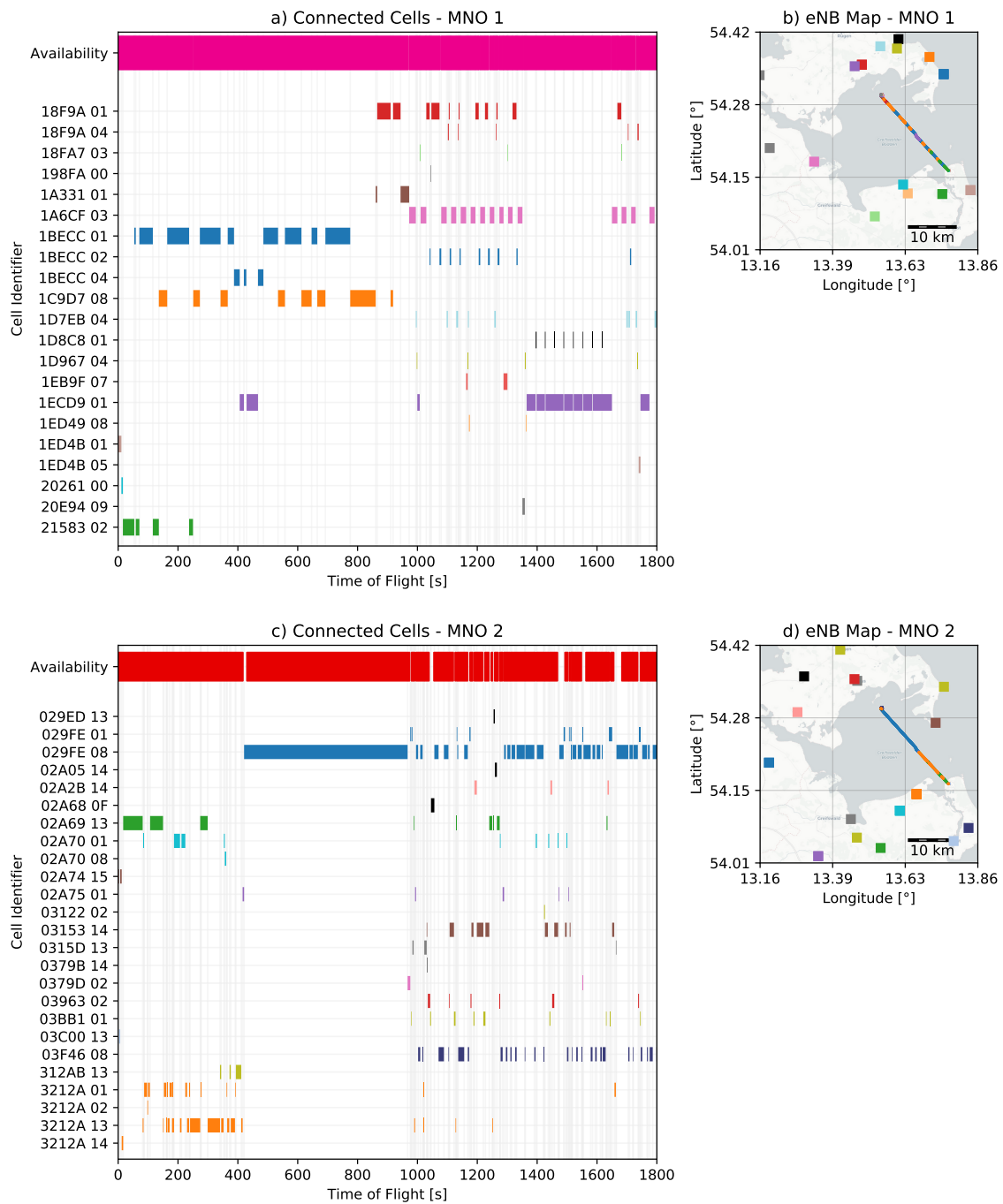


Figure 12. Evaluation of the LTE connectivity of the first part of Peenemünde long range flight. The top row (subplots a and b) reflects MNO 1, the bottom row (c,d) MNO 2. The first column (a,c) indicates the cell identifier to which the UAS is currently connected to. The second column (b,d) shows a map of the eNB locations as well as the trajectory of the UAV. The respective color represents the association with an eNB, which may have multiple sectors and/or frequencies, which are distinguishable by the cell identifier. Data set [2a].

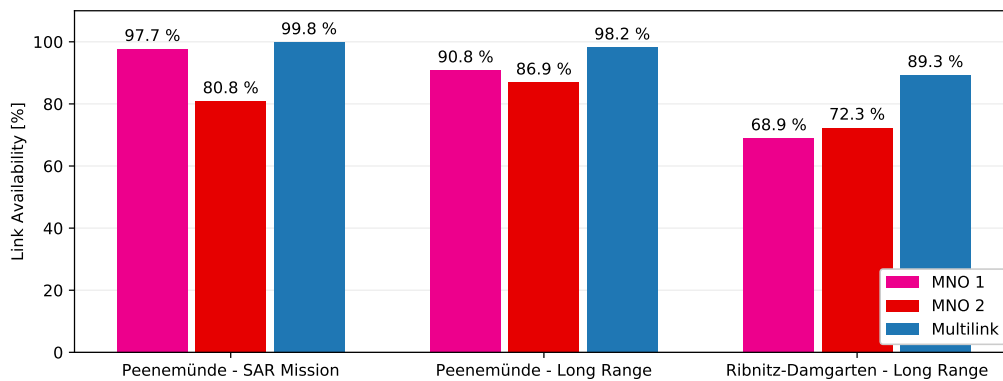


Figure 13. Evaluation of link availability during long range flight shows the benefits of the proposed multi-link strategy. Flight data sets [2a] [2b] [5].

6. Evaluation of Multi-Link Empowered Link Availability Improvement

The following section shows the benefits of the proposed multi-link strategy in terms of link quality and availability improvement. *Availability* within the scope of this section means that the communication link is able to transmit data between the UAS and the ground station. For safe and reliable flight operations, reliable communication is mandatory at all times. Despite packet loss occurring only rarely due to LTE's HARQ mechanism, the communication link may be unavailable if there is no available eNB to connect to, the signal quality is too bad, or the LTE modem is performing a handshake between two eNBs. To assess the system's performance, the data of long-range flights in Peenemünde [2] and Ribnitz-Damgarten [5] are analyzed and evaluated. Therefore, after discussing the benefits of link quality improvement due to the multi-link architecture, the subsequent passage first describes availability calculation methodology and afterwards evaluates and discusses multi-link empowered link availability gains.

Figure 14 exemplifies the benefits of the heterogeneous link aggregation to the overall link quality based on the example of the first half hour of Peenemünde long-range flight [2a]. The figure shows a time series of the SINR signal quality over time for both MNOs. Raw samples are plotted in the background, the bold lines show a post-processed moving average of 10 s. As discussed previously, SINR values below 0 dB indicate the worst channel conditions. However, the plot shows that most of the time when one MNO suffers from bad channel quality, the other operator is able to assist. This effect can be seen for a long duration of several minutes, e.g., during a time of flight between 500 s and 900 s. In general, one can say that the more heterogeneous the links are, the more gain the multi-link approach yields.

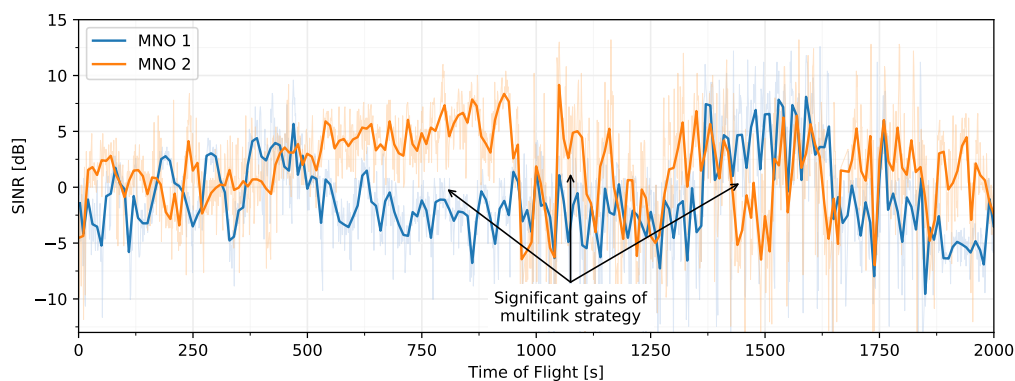


Figure 14. Benefits of heterogeneous multi-link aggregation: When SINR falls below 0 dB, the communication link may be heavily degraded. The proposed approach boosts performance, especially when one link is good while the other is bad. Data set [2a].

In the next step, the availability of both MNOs is evaluated. To achieve this, Round Trip Time (RTT) measurements were conducted. Internet Control Message Protocol (ICMP) messages were sent over each communication link targeting the ground control station with a static frequency of 2 Hz and a fixed packet size of 64 Bytes. This approach allows measuring communication link latency as well as packet losses while at the same time exposing minimal impact on the link performance. Within the scope of the underlying evaluation, a link is defined as available, when (a) a minimum of one ICMP packet was successfully echoed by the ground control station, and (b) the respective RTT of the packet was below or equal to 1 s. The availability for each link, therefore, refers to the ratio of time of flight in which the UAS was able to communicate with the ground control via that link. The final multi-link availability results from the combination of individual communication channels: If at least one of the single links is available, the multi-link is also, if no single link is, the multi link is also unavailable.

Figure 15 shows a time-series example of the link availability evaluation taken from the Peenemünde long-range flight. The first two rows represent two public German MNOs, the bottom row features the resulting multi-link. Whenever the bars are colored, the communication link is available. White gaps indicate that no connectivity and no data can be transmitted. Shorter gaps are typically caused by non-beneficial handovers between different cells and last only a few seconds. Larger gaps originate from network unavailability and bad channel conditions.

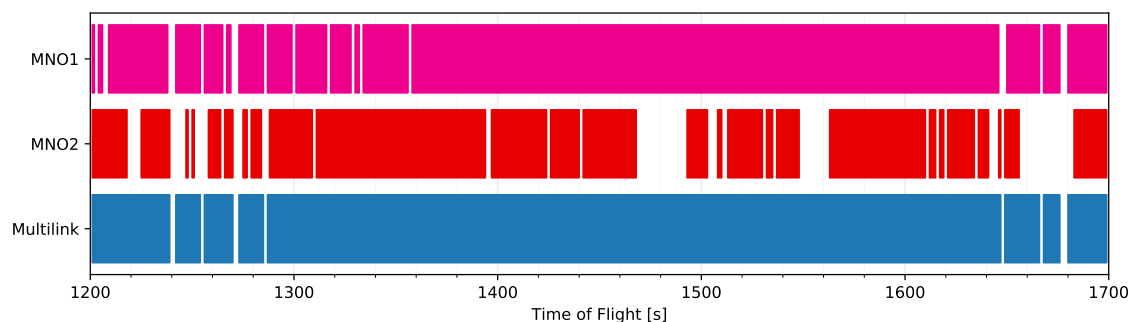


Figure 15. Example of link availability increase by using multiple public MNOs. Shorter outages occur due to non-seamless handovers between two LTE cells, larger outages are caused by general network unavailability. The multi-link approach enhances overall link availability. Excerpt from Peenemünde long range flight data set [2a].

The overall increase in availability is provided in the statistical evaluation in Figure 13 for the multi-link UAV scenarios [2a] [2b] [5]. The multi-link approach yields the highest availability in all scenarios. For Peenemünde SAR Mission, 99.8% availability was achieved, which is primarily because the mission was flown in the proximity of the shore, where MNO 1 had a good single link performance of 97.7%. Nevertheless, in the Peenemünde long-range scenario, the multi-link performed very well with a similar score of 98.2%. Here, the single link availability of 90.8% of MNO 1 was lower than in the previous flight. In the Ribnitz-Damgarten scenario, both MNO's single link performances were significantly lower than in the Peenemünde scenarios. This is due to the fact that the Ribnitz-Damgarten site is more rural and less populated and contains fewer surrounding LTE coverage. Nevertheless, the multi-link approach results in the highest availability of 89.3%, which is an increase of 20% for MNO 1 and 17% for MNO 2. In conclusion, it can be stated that the multi-link approach increases the availability in all scenarios.

7. Overall Application Layer Performance Evaluation

In the following section, the multi-link approach is assessed from the application layer perspective. The multi-link aggregation is performed using the MPTCP transport player protocol. MPTCP works transparently for the application layer and enables smooth and seamless handovers between different links and interfaces, e.g., when one link is unavailable.

Figure 16 shows a time-series evaluation of the effective throughput of the UAV during Peenemünde flights [2]. The throughput was recorded at the UAV using the open source software *Bandwidth Monitor NG (bwm-ng)*, which captures the data rates for each interface. Throughout the experiment, the MPTCP scheduler “Lowest Round-Trip-Time First (LRF)” was used. The plot shows the data rates for the public MNOs 1 and 2 as well as for a local dedicated LTE network and the total payload data rate. The bold lines represent a rolling mean of 5 s of the raw samples (thin lines). The dedicated LTE is a small cell solution located at the airport to allow easy maintenance when the UAV is at the airport, where public MNO coverage is not always available—especially in shadowing of buildings. Due to the transparent nature of MPTCP, in the future, this LTE small cell can be replaced by a full long-range LTE solution, which could assist as a third aerial data link. During the experiments, a video stream with an approximate data rate of 500 kbps as well as telemetry and control messages with approx. 100 kbps (including the previously described ICMP packets) were transmitted. The plot illustrates the smooth handover between the data links, which is enabled by MPTCP. When one link is unavailable, data is outsourced on the other link.

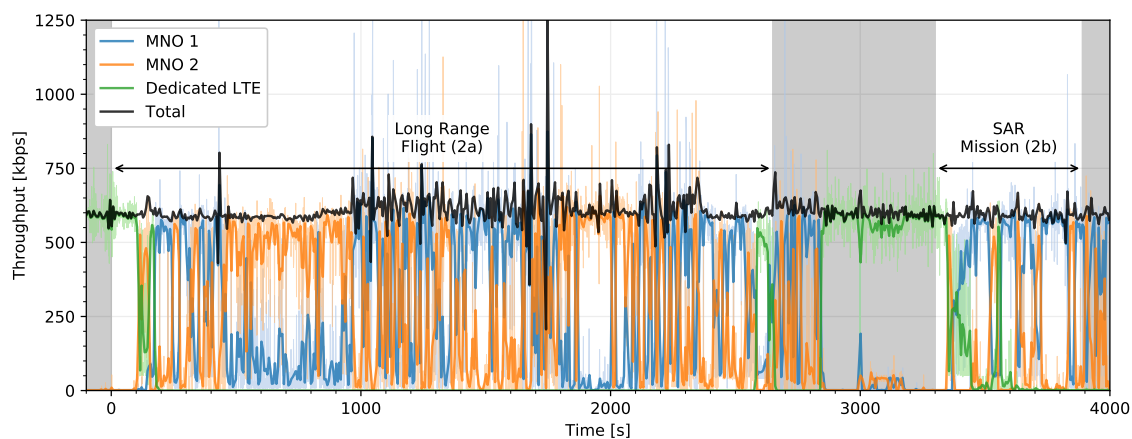


Figure 16. Evaluation of throughput over time for the Peenemünde flight tests [2]. A live video stream payload (~500 kbps) and telemetry and control messages (~100 kbps) were continuously streamed from the UAV to the ground. MPTCP handles seamless and smooth handovers between different networks. Data set [2].

Another important key performance indicator for aerial communication is latency. As previously described, ICMP data packets were used to trace the communication links availability and RTT. Figure 17 shows a time-series evaluation of the RTT measurement (a) as well as a histogram with the PDF. The bold lines represent again a moving average of 5 s of the raw data (thin lines). Taking the logarithmic representation of the y-axis of the time-series plot into account, it can be seen that despite some spikes latency resides most of the time below 80 ms. Average (median) RTT for MNO 1 is with 45.4 ms comparable to MNO 2’s slightly better performance of 41.3 ms. With 80% percentiles of 58.5 ms (MNO 1) and 56.0 ms (MNO 2), the latency for both public MNO is below 60 ms. However, when considering the 99th quantile, the upper bounds are 11,223.0 ms for MNO 1 and 6788.0 ms for MNO 2.

During the UAV experiments (all data sets except [4]) the communication links were not maxed out to avoid interferences on the video stream and telemetry and control data flows. In order to assess maximum throughput performance, a manned flight was conducted (dataset [5]). Figure 18 presents the evaluation of the experiment. The left subplot (a) illustrates the throughput over each individual link as well as the sum of all links. Subplot (b) shows the statistical boxplot evaluation. To evaluate maximum performance, an *iPerf*-like set-up was used: over a TCP socket randomly generated data was sent. Whenever sending was possible the data was sent over the socket. The outgoing buffer was always filled. Again, the *bwm-ng* tool was used to record the throughput for each interface.

During the experiment, no *useful* payload (e.g., video stream or telemetry and control data) was transmitted, which is contrary to the previous experiments. MNO 1 achieved with 10.6 Mbps a higher throughput than MNO 2 with 6.6 Mbps during the experiments. The peak data rate was 42 Mbps for the single links, being the rare exception right at the beginning of the flight. The theoretic maximum achievable throughput in LTE uplink with the underlying hardware is at 50 Mbps. The first part of this manned flight is comparable to the route of Peenemünde long-range flight [2]. Afterwards, the network performance in direction to the Polish border has been evaluated, where network coverage of the German MNOs was not always given. As the antennas were mounted in flight direction, improved performance is assumed with an optimized antenna positioning. On the way back, when approaching Peenemünde airport, the MNO 2 LTE modem tried to attach to a Polish MNO several times. However, the roaming attempts were unsuccessful. MNO 1 recovered and maintained a good throughput of ~20 Mbps. Despite being in MNO 2 network coverage, the LTE modem of MNO 2 was unable to directly reattach to the network and pick up service. The flight was completed performing SAR search patterns similar to Peenmünde flight [2b].

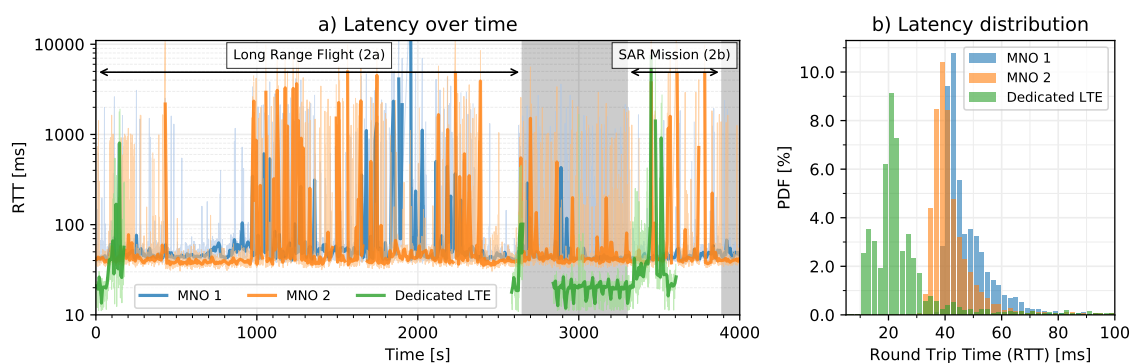


Figure 17. Evaluation of the latency key-performance indicator based on ICMP RTT measurements over each individual data link. Data sets [2].

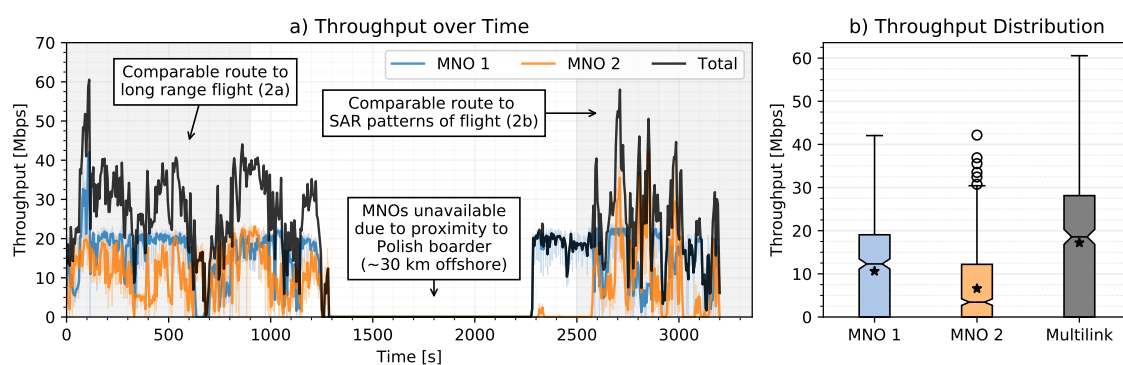


Figure 18. Maximum application layer throughput during *manned* flight show LTE maritime network performance. Dataset [4].

Excluding the gap at the Polish border, the overall throughput performance was very good. MPTCP enables a smooth and transparent handover between different communication links. The data rate is sufficient to transfer high data payload like video streams, high-resolution camera images as well as telemetry and control data.

8. Conclusions

Within the scope of this paper, a reliable long range multi-link communication system for unmanned aerial search and rescue missions has been proposed. The proposed system architecture has been implemented and the communication module leverages multiple LTE modems and networks

together with **MPTCP** for multi link aggregation. The system has been evaluated in several flight tests using an **UAS** in several scenarios and all recorded data sets have been published alongside this publication. The evaluation of the datasets provides a comparison of the network channel quality in the air in comparison to ground-based measurements: Aerial conditions are worse than ground-based conditions as public networks are not optimized for **UAS**. However, it could be shown that channel models can provide a more accurate path loss estimate due to less shadowing effects in channel propagation of the **UAS**. By measuring the **RTT** of all communication links, the evaluation has shown that the proposed multi-link strategy can significantly increase the communication link availability in maritime scenarios. The multi-link approach also enables smooth handovers between different networks. This allows seamless streaming of constant bitrate payloads like video streams. In a supplementary measurement campaign, a manned plane has been used to investigate the maximum data rate of the system without interfering with the **UAS**'s stability. The experiments underline the benefits of **MPTCP**: the average and maximum throughput is significantly increased in comparison to single link scenarios. For future work, satellite-based Internet will be included in the multi-link maritime scenarios as well as the multi-link approach will be integrated in a multi-link system to be used for mixed vehicle (ground and aerial) rescue robotics scenarios. In those future scenarios, 5G and WiFi6 links will also be considered.

Author Contributions: Conceptualization: C.W. and J.T.; methodology: C.W., J.G., and J.T.; software: M.P., P.G., F.E., and J.G.; formal analysis, J.G. and J.T.; investigation: M.P., P.G., F.E., F.K., and J.G.; data curation: J.G.; writing: J.G.; visualization: J.T. and J.G.; supervision and project administration: J.T., C.W. All authors have read and agreed to the published version of the manuscript.

Funding: This work has been supported by German Federal Ministry of Education and Research (BMBF) for the projects LARUS (Supporting Maritime Search and Rescue Missions with Unmanned Aircraft Systems, 13N14133) and A-DRZ (Establishment of the German Rescue Robotics Center, 13N14857) as well as the Deutsche Forschungsgemeinschaft (DFG) within the Collaborative Research Center SFB 876 "Providing Information by Resource-Constrained Analysis", projects A4 and B4.

Acknowledgments: We would like to thank all partners of the LARUS project for their excellent cooperation, in the context of the experiments especially Thomas Lübcke and the voluntary workers of the DGzRS for their contribution to the SAR experiments, Michael Schmidt and Stefan Flemming (HAVS) for provisioning of the UAS and implementation of the communication equipment inside of the plane; Thomas Lamla for the airport access; Robert Falkenberg (TU Dortmund), Bundesnetzagentur and Telekom Deutschland for providing the SAR BOS LTE frequency for the dedicated LTE network. Veronika Pillmann for her support in grammar and spell checking.

Conflicts of Interest: The authors declare no conflict of interest.

Abbreviations

The following abbreviations are used in this manuscript:

ADMIT	quAlity-Driven Multipath TCP
BVLOS	Beyond Visual Line of Sight
Cell ID	Cell Identifier
DASH	Dynamic Adaptive Streaming over HTTP
EIRP	Effective Isotropic Radiated Power
eNB	enhanced NodeB
FPV	First-Person View
GUI	Graphical User Interface
HARQ	Hybrid Automatic Repeat Request
HD	High Definition
HTTP	Hypertext Transfer Protocol
ICAO	International Civil Aviation Organization
ICMP	Internet Control Message Protocol
LOS	Line of Sight
LTE	Long Term Evolution
MCTCP	Multi-Connection TCP
MMTCP	Maximum Multipath TCP
MNO	Mobile Network Operator
MPQUIC	Multipath QUIC
MPTCP	Multipath TCP
MPUDP	Multipath UDP
MRCC	Maritime Rescue and Control Center
NASA	National Aeronautics and Space Administration

NLOS	Non-Line of Sight
PDF	Probability Density Function
QoS	Quality of Service
QUIC	Quick UDP Internet Connections
RSRP	Reference Signal Received Power
RSRQ	Reference Signal Received Quality
RSSI	Received Signal Strength Indicator
RTMP	Real-Time Messaging Protocol
RTT	Round Trip Time
SAR	Search and Rescue
SCTP	Stream Control Transmission Protocol
SINR	Signal-to-Interference-plus-Noise Ratio
TCP	Transmission Control Protocol
UAS	Unmanned Aircraft System
UAV	Unmanned Aerial Vehicle
UDP	User Datagram Protocol
UE	User Equipment
VPN	Virtual Private Network
WLAN	Wireless Local Area Network

References

1. LARUS Research Project Website. 2019. Available online: <http://larus.kn.e-technik.tu-dortmund.de> (accessed on 21 January 2020).
2. Video of the LARUS Project. 2020 Available online: <https://www.youtube.com/watch?v=kJ9ABk8Rr4M> (accessed on 10 March 2020).
3. Shakhathreh, H.; Sawalmeh, A.H.; Al-Fuqaha, A.; Dou, Z.; Almaita, E.; Khalil, I.; Othman, N.S.; Khreishah, A.; Guizani, M. Unmanned Aerial Vehicles (UAVs): A Survey on Civil Applications and Key Research Challenges. *IEEE Access* **2019**, *7*, 48572–48634. [[CrossRef](#)]
4. Cubber, G.D.; Doroftei, D.; Rudin, K.; Berns, K.; Matos, A.; Serrano, D.; Sanchez, J.; Govindaraj, S.; Bedkowski, J.; Roda, R.; et al. Introduction to the Use of Robotic Tools for Search and Rescue. In *Search and Rescue Robotics*; IntechOpen: London, UK, 2017; Chapter 1. [[CrossRef](#)]
5. Lygouras, E.; Santavas, N.; Taitzoglou, A.; Tarchanidis, K.; Mitropoulos, A.; Gasteratos, A. Unsupervised Human Detection with an Embedded Vision System on a Fully Autonomous UAV for Search and Rescue Operations. *Sensors* **2019**, *19*, 3542. [[CrossRef](#)] [[PubMed](#)]
6. Seguin, C.; Blaqui ere, G.; Loundou, A.; Michelet, P.; Markarian, T. Unmanned aerial vehicles (drones) to prevent drowning. *Resuscitation* **2018**, *127*, 63–67, [[CrossRef](#)] [[PubMed](#)]
7. P lka, M.; Ptak, S.; Kuziora,  .; Kuczyńska, A. The Use of Unmanned Aerial Vehicles by Urban Search and Rescue Groups. In *Drones*; Dekoulis, G., Ed.; IntechOpen: London, UK, 2018; Chapter 6. [[CrossRef](#)]
8. Roberts, J.; Frousheger, D.; Williams, B.; Campbell, D.; Walker, R. How the Outback Challenge Was Won: The Motivation for the UAV Challenge Outback Rescue, the Competition Mission, and a Summary of the Six Events. *IEEE Robot. Autom. Mag.* **2016**, *23*, 54–62. [[CrossRef](#)]
9. Marques, M.M.; Dias, P.; Santos, N.P.; Lobo, V.; Batista, R.; Salgueiro, D.; Aguiar, A.; Costa, M.; da Silva, J.E.; Ferreira, A.S.; et al. Unmanned aircraft systems in maritime operations: Challenges addressed in the scope of the SEAGULL project. In Proceedings of the OCEANS 2015—Genova, Genoa, Italy, 18–21 May 2015; pp. 1–6. [[CrossRef](#)]
10. Volkert, A.; Hackbarth, H.; Lieb, T.J.; Kern, S. Flight Tests of Ranges and Latencies of a Threefold Redundant C2 Multi-Link Solution for Small Drones in VLL Airspace. In Proceedings of the 2019 Integrated Communications, Navigation and Surveillance Conference (ICNS), Herndon, VA, USA, 9–11 April 2019; pp. 1–14. [[CrossRef](#)]
11. Fragkos, G.; Tsiropoulou, E.E.; Papavassiliou, S. Disaster Management and Information Transmission Decision-Making in Public Safety Systems. In Proceedings of the 2019 IEEE Global Communications Conference (GLOBECOM), Waikoloa Village, HI, USA, 9–13 December 2019; pp. 1–6.
12. Ponchak, D.S.; Templin, F.L.; Sheffield, G.; Taboso, P.; Jain, R. Reliable and secure surveillance, communications and navigation (RSCAN) for Unmanned Air Systems (UAS) in controlled airspace. In Proceedings of the 2018 IEEE Aerospace Conference, Big Sky, MT, USA, 3–10 March 2018; pp. 1–14. [[CrossRef](#)]

13. Apaza, R.D.; Popescu, L. The way to the future has already started: ICAO Aeronautical Telecommunication Network (ATN) using Internet Protocol Suite (IPS) Standards and Protocol evolution update. In Proceedings of the 2018 IEEE/AIAA 37th Digital Avionics Systems Conference (DASC), London, UK, 23–27 September 2018; pp. 1–6. [\[CrossRef\]](#)
14. Azari, M.M.; Rosas, F.; Pollin, S. Cellular Connectivity for UAVs: Network Modeling, Performance Analysis, and Design Guidelines. *IEEE Trans. Wirel. Commun.* **2019**, *18*, 3366–3381. [\[CrossRef\]](#)
15. Raiciu, C.; Paasch, C.; Barre, S.; Ford, A.; Honda, M.; Duchene, F.; Bonaventure, O.; Handley, M. How Hard Can It Be? Designing and Implementing a Deployable Multipath TCP. In Proceedings of the 9th USENIX Symposium on Networked Systems Design and Implementation (NSDI 12), San Jose, CA, USA, 25–27 April 2012; pp. 399–412.
16. Jagetiya, A.; Rama Krishna, C.; Haider, Y. Survey of Transport Layer Multihoming Protocols and Performance Analysis of MPTCP. In Proceedings of the 2nd International Conference on Communication, Computing and Networking, Chandigarh, India, 29–30 March 2018; Krishna, C.R., Dutta, M., Kumar, R., Eds.; Springer: Singapore, 2019; pp. 15–24.
17. Guanhua Ye.; Saadawi, T.N.; Myung Lee. IPCC-SCTP: An enhancement to the standard SCTP to support multi-homing efficiently. In Proceedings of the IEEE International Conference on Performance, Computing, and Communications, Phoenix, AZ, USA, 15–17 April 2004; pp. 523–530. [\[CrossRef\]](#)
18. Abrahamsson, H.; Abdesslem, F.B.; Ahlgren, B.; Brunstrom, A.; Marsh, I.; Björkman, M. Connected Vehicles in Cellular Networks: Multi-Access Versus Single-Access Performance. In Proceedings of the 2018 Network Traffic Measurement and Analysis Conference (TMA), Vienna, Austria, 26–29 June 2018; pp. 1–6. [\[CrossRef\]](#)
19. Scharf, M.; Banniza, T. MCTCP: A Multipath Transport Shim Layer. In Proceedings of the 2011 IEEE Global Telecommunications Conference—GLOBECOM 2011, Houston, TX, USA, 5–9 December 2011; pp. 1–5. [\[CrossRef\]](#)
20. Hesmans, B.; Duchene, F.; Paasch, C.; Detal, G.; Bonaventure, O. Are TCP Extensions Middlebox-Proof? In Proceedings of the 2013 Workshop on Hot Topics in Middleboxes and Network Function Virtualization, HotMiddlebox '13, Santa Barbara, CA, USA, 9 December 2013; Association for Computing Machinery: New York, NY, USA, 2013; pp. 37–42. [\[CrossRef\]](#)
21. Khalili, R.; Gast, N.; Popovic, M.; Le Boudec, J.Y. MPTCP is Not Pareto-Optimal: Performance Issues and a Possible Solution. *IEEE/ACM Trans. Netw.* **2013**, *21*, 1651–1665. [\[CrossRef\]](#)
22. Kheirkhah, M.; Wakeman, I.; Parisi, G. MMPTCP: A multipath transport protocol for data centers. In Proceedings of the IEEE INFOCOM 2016—The 35th Annual IEEE International Conference on Computer Communications, San Francisco, CA, USA, 10–15 April 2016; pp. 1–9. [\[CrossRef\]](#)
23. Lukaszewski, D.; Xie, G. Multipath Transport for Virtual Private Networks. In Proceedings of the 10th USENIX Workshop on Cyber Security Experimentation and Test (CSET 17), USENIX Association, Vancouver, BC, Canada, 14 August 2017.
24. Behnke, D.; Priebe, M.; Rohde, S.; Heimann, K.; Wietfeld, C. ScalaNC—Scalable heterogeneous link aggregation enabled by Network Coding. In Proceedings of the 13th IEEE International Conference on Wireless and Mobile Computing, Networking and Communications (WiMob 2017)—Fourth International Workshop on Emergency Networks for Public Protection and Disaster Relief (EN4PPDR'17). Rome, Italy, 9–11 October 2017.
25. Cloud, J.; du Pin Calmon, F.; Zeng, W.; Pau, G.; Zeger, L.M.; Medard, M. Multi-Path TCP with Network Coding for Mobile Devices in Heterogeneous Networks. In Proceedings of the 2013 IEEE 78th Vehicular Technology Conference (VTC Fall), Las Vegas, NV, USA, 2–5 September 2013; pp. 1–5. [\[CrossRef\]](#)
26. Wu, J.; Yuen, C.; Cheng, B.; Wang, M.; Chen, J. Streaming High-Quality Mobile Video with Multipath TCP in Heterogeneous Wireless Networks. *IEEE Trans. Mobile Comput.* **2016**, *15*, 2345–2361. [\[CrossRef\]](#)
27. Hayes, B.; Chang, Y.; Riley, G. Adaptive bitrate video delivery using HTTP/2 over MPTCP architecture. In Proceedings of the 2017 13th International Wireless Communications and Mobile Computing Conference (IWCMC), Valencia, Spain, 26–30 June 2017; pp. 68–73. [\[CrossRef\]](#)
28. Jung, W.S.; Yim, J.; Ko, Y.B. Adaptive offloading with MPTCP for unmanned aerial vehicle surveillance system. *Ann. Telecommun.* **2018**, *73*, 613–626. [\[CrossRef\]](#)
29. Khatouni, A.S.; Marsan, M.A.; Mellia, M.; Rejaie, R. Adaptive schedulers for deadline-constrained content upload from mobile multihomed vehicles. In Proceedings of the 2017 IEEE International Symposium on Local and Metropolitan Area Networks (LANMAN), Osaka, Japan, 12–14 June 2017; pp. 1–6. [\[CrossRef\]](#)

30. Khatouni, A.S.; Marsan, M.A.; Mellia, M.; Rejaie, R. Deadline-constrained content upload from multihomed devices: Formulations and algorithms. *Comput. Netw.* **2018**, *142*, 76–92. [[CrossRef](#)]
31. Chiba, N.; Ogura, M.; Nakamura, R.; Hadama, H. Dual transmission protocol for video signal transfer for real-time remote vehicle control. In Proceedings of the 20th Asia-Pacific Conference on Communication (APCC2014), Pattaya, Thailand, 1–3 October 2014; pp. 315–320. [[CrossRef](#)]
32. Google. Chromium QUIC Implementation. Available online: <https://cs.chromium.org/chromium/src/net/quic/> (accessed on 27 March 2020).
33. Langley, A.; Riddoch, A.; Wilk, A.; Vicente, A.; Krasic, C.; Zhang, D.; Yang, F.; Kouranov, F.; Swett, I.; Iyengar, J.; et al.. The QUIC Transport Protocol: Design and Internet-Scale Deployment. In Proceedings of the Conference of the ACM Special Interest Group on Data Communication, SIGCOMM '17, Los Angeles, CA, USA, 21–25 August 2017. Association for Computing Machinery: New York, NY, USA, 2017; pp. 183–196. [[CrossRef](#)]
34. De Coninck, Q.; Bonaventure, O. Multipath QUIC: Design and Evaluation. In Proceedings of the 13th International Conference on Emerging Networking EXperiments and Technologies, CoNEXT '17, Incheon, Korea, 12–15 December 2017; Association for Computing Machinery: New York, NY, USA, 2017; pp. 160–166. [[CrossRef](#)]
35. Viernickel, T.; Froemmgen, A.; Rizk, A.; Koldehofe, B.; Steinmetz, R. Multipath QUIC: A Deployable Multipath Transport Protocol. In Proceedings of the 2018 IEEE International Conference on Communications (ICC), Kansas City, MO, USA, 20–24 May 2018; pp. 1–7. [[CrossRef](#)]
36. Mogensen, R.S.; Markmoller, C.; Madsen, T.K.; Kolding, T.; Pocovi, G.; Lauridsen, M. Selective Redundant MP-QUIC for 5G Mission Critical Wireless Applications. In Proceedings of the 2019 IEEE 89th Vehicular Technology Conference (VTC2019-Spring), Kuala Lumpur, Malaysia, 28 April–1 May 2019; pp. 1–5. [[CrossRef](#)]
37. Paasch, C.; Ferlin, S.; Alay, O.; Bonaventure, O. Experimental Evaluation of Multipath TCP Schedulers. In Proceedings of the 2014 ACM SIGCOMM Workshop on Capacity Sharing Workshop, CSWS '14, Chicago, IL, USA, 17–22 August 2014; Association for Computing Machinery: New York, NY, USA, 2014; pp. 27–32. [[CrossRef](#)]
38. Paasch, C.; Detal, G.; Duchene, F.; Raiciu, C.; Bonaventure, O. Exploring Mobile/WiFi Handover with Multipath TCP. In Proceedings of the 2012 ACM SIGCOMM Workshop on Cellular Networks: Operations, Challenges, and Future Design, Association for Computing Machinery, CellNet '12, New York, NY, USA, 13 August 2012; pp. 31–36. [[CrossRef](#)]
39. Chirwa, R.M.N.; Lauf, A.P. Performance improvement of transmission in Unmanned Aerial Systems using multipath TCP. In Proceedings of the 2014 IEEE International Symposium on Signal Processing and Information Technology (ISSPIT), Noida, India, 15–17 December 2014; pp. 19–24. [[CrossRef](#)]
40. Frommgen, A.; Erbhäufel, T.; Buchmann, A.; Zimmermann, T.; Wehrle, K. ReMP TCP: Low latency multipath TCP. In Proceedings of the 2016 IEEE International Conference on Communications (ICC), Kuala Lumpur, Malaysia, 23–26 May 2016; pp. 1–7. [[CrossRef](#)]
41. Frömmgen, A.; Rizk, A.; Erbhäuundefinder, T.; Weller, M.; Koldehofe, B.; Buchmann, A.; Steinmetz, R. A Programming Model for Application-Defined Multipath TCP Scheduling. In Proceedings of the 18th ACM/IFIP/USENIX Middleware Conference, Middleware '17, Newport Beach, CA, USA, 26–30 November 2017; Association for Computing Machinery: New York, NY, USA, 2017; pp. 134–146. [[CrossRef](#)]
42. Khuwaja, A.A.; Chen, Y.; Zhao, N.; Alouini, M.; Dobbins, P. A Survey of Channel Modeling for UAV Communications. *IEEE Commun. Surv. Tutor.* **2018**, *20*, 2804–2821. [[CrossRef](#)]
43. Huang, F.; Liao, X.; Bai, Y. Multipath channel model for radio propagation over sea surface. *Wirel. Pers. Commun.* **2016**, *90*, 245–257. [[CrossRef](#)]
44. Park, M.; Seo, H.; Park, P.; Kim, Y.; Jeong, J. LTE maritime coverage solution and ocean propagation loss model. In Proceedings of the 2017 International Conference on Performance Evaluation and Modeling in Wired and Wireless Networks (PEMWN), Paris, France, 28–30 November 2017; pp. 1–5.
45. Matolak, D.W.; Sun, R. Air–Ground Channel Characterization for Unmanned Aircraft Systems—Part I: Methods, Measurements, and Models for Over-Water Settings. *IEEE Trans. Veh. Technol.* **2016**, *66*, 26–44. [[CrossRef](#)]
46. Miller, A.; Brown, R.; Vegh, E. *New Derivation for the Rough-Surface Reflection Coefficient and for the Distribution of Sea-Wave Elevations*; ET: London, UK, 1984; Volume 131, pp. 114–116. [[CrossRef](#)]

47. Parsons, J.D. *The Mobile Radio Propagation Channel*; Wiley Online Library: Hoboken, NJ, USA, 2000.
48. Vaughan, R.; Andersen, J.B. *Channels, Propagation and Antennas for Mobile Communications*; IET: London, UK, 2003; Volume 50.
49. Gldenring, J.; Koring, L.; Gorczak, P.; Wietfeld, C. Heterogeneous Multilink Aggregation for Reliable UAV Communication in Maritime Search and Rescue Missions. In Proceedings of the 15th IEEE International Conference on Wireless and Mobile Computing, Networking and Communications (WiMob 2019)–Sixth International Workshop on ICT Systems for Public Protection and Risk Reduction–2019 (ICT4PPRR’19), Barcelona, Spain, 21 October 2019; IEEE: Piscataway, NJ, USA, 2019.
50. Paasch, C.; Barre, S. Multipath TCP implementation in the Linux Kernel. Available online: <http://www.multipath-tcp.org> (accessed on 27 March 2020).
51. gstreamer Open Source Multimedia Framework. Available online: <https://gstreamer.freedesktop.org> (accessed on 27 March 2020).
52. OBS Open Broadcaster Software (OBS) Studio. Available online: <https://obsproject.com> (accessed on 27 March 2020).
53. Holma, H.; Toskala, A., UTRAN Long-Term Evolution. In *WCDMA for UMTS: HSPA Evolution and LTE*; Wiley: Hoboken, NJ, USA, 2010. [CrossRef]
54. Tiemann, J.; Feldmeier, O.; Wietfeld, C. Supporting Maritime Search and Rescue Missions through UAS-based Wireless Localization. In Proceedings of the IEEE Global Communications Conference Workshops (GLOBECOM Workshops), 9th International Workshop on Wireless Networking and Control of Unmanned Autonomous Vehicles (Wi-UAV), Abu Dhabi, United Arab Emirates, 9–13 December 2018. [CrossRef]
55. Singhal, C.; De, S.; Tsiropoulou, E.E.; Vamvakas, P.; Papavassiliou, S. *Resource Allocation in Next-Generation Broadband Wireless Access Networks*; IGI Global: Hershey, PA, USA, 2017.



© 2020 by the authors. Licensee MDPI, Basel, Switzerland. This article is an open access article distributed under the terms and conditions of the Creative Commons Attribution (CC BY) license (<http://creativecommons.org/licenses/by/4.0/>).